communications biology

A Nature Portfolio journal

Article

https://doi.org/10.1038/s42003-025-09424-7

Sae2 integrates CDK and checkpoint phosphorylation to coordinate MRX cleavage with checkpoint attenuation

Erika Casari[1,2], Marco Gnugnoli[1,2], Paolo Pizzul[1], Renata Tisi[1] & Maria Pia Longhese[1]

Yeast Sae2 plays a dual role in the DNA damage response by suppressing Rad53 activation and stimulating DNA end clipping via the MRX complex. Using AlphaFold3-based modeling and mutational analysis, here we show that Mec1/Tel1-dependent phosphorylation of Sae2 at T90 or T279 is sufficient to restrain Rad9-Rad53 interaction and Rad53 kinase activation. Cells expressing a non-phosphorylatable Sae2 double mutant (T90A T279A) display persistent Rad53 activation, whereas phosphomimetic Sae2 variants (T90E or T279E) restore normal checkpoint inactivation. Structural modeling and charge-reversal genetics indicate that electrostatic interactions between phosphorylated T90/T279 of Sae2 and Rad53 residue R70 are critical for this regulation. In addition, T279 phosphorylation, but not T90, cooperates with cyclin-dependent kinase (CDK)-dependent phosphorylation of Sae2 S267 to promote MRX-dependent resolution of hairpin DNA structures and processing of meiotic double-strand breaks (DSBs). A Sae2 T279E phosphomimetic partially rescues both hairpin cleavage defects and DNA damage sensitivity of *tel1*Δ cells, indicating that Tel1 promotes MRX activity primarily through Sae2 T279 phosphorylation.

DNA double-strand breaks (DSBs) represent one of the most hazardous forms of DNA damage, as they can lead to genomic instability if not properly repaired. In eukaryotic cells, DSB repair occurs via two main pathways: non-homologous end joining (NHEJ)[1], a rapid but error-prone mechanism, and homologous recombination (HR)[2], a more accurate pathway that requires the generation of 3′ single-stranded DNA (ssDNA) overhangs through a process known as DNA end resection[3]. This process is initiated by an endonucleolytic incision of the 5′-ending strand at a short distance from the DNA terminus, which is catalyzed by the evolutionarily conserved Mre11-Rad50-Xrs2/NBS1 complex (MRX in *S. cerevisiae*, MRN in mammals)[4–7]. The Mre11 subunit exhibits both 3′–5′ exonuclease and endonuclease activities[8–10], while Rad50 functions as an ATPase[11,12]. Following the initial clipping event, MRX catalyzes 3′–5′ exonucleolytic degradation toward the DNA end. Long-range resection in the 5′–3′ direction is then carried out by either the Exo1 nuclease or the Dna2 nuclease in cooperation with the Sgs1/BLM helicase[13,14].

The MRX-mediated incision is crucial when DNA ends are obstructed by protein adducts or covalent modifications, such as hairpin-capped DNA ends, covalent DNA-topoisomerase complexes, or meiotic DSBs covalently bound by Spo11[4,15,16]. Conversely, MRX is not required for the processing of clean DNA breaks, such as those produced by endonucleases, where Exo1 or Dna2-Sgs1 can directly initiate resection[17].

In both yeast and mammals, Mre11 endonuclease activity requires the ATPase function of Rad50 and the presence of Sae2 (CtIP in humans), which stimulates Mre11 endonuclease activity within the context of the MRX complex[18–20]. In the ATP-bound state, the Rad50 dimer forms a DNA-binding platform that sterically hinders Mre11 access to double-stranded DNA (resting state). ATP hydrolysis triggers dissociation of Rad50 nucleotide-binding domains, allowing Mre11 subunits to reposition and access DNA for cleavage (cutting state)[21–25]. Mre11 nuclease activity requires the binding of Sae2 with Rad50[18], which is thought to stabilize the nucleolytically active Mre11-Rad50 conformation[26,27].

The generation of DNA DSBs also elicits a checkpoint response, whose key players are the apical protein kinases Tel1 and Mec1, as well as their mammalian orthologs ATM and ATR, respectively[28]. Upon DSB recognition, Tel1 and Mec1 transduce checkpoint signals to the downstream effector kinases Rad53 and Chk1 (CHK2 and CHK1 in mammals, respectively), whose activation requires Rad9 (53BP1 in mammals). Rad9 serves as the proximal adapter and scaffold for Rad53 activation. In response to DNA damage, Mec1 and Tel1 phosphorylate Rad9 at multiple sites; these modifications promote Rad9 multimerization and create docking sites for Rad53 binding[29–33]. Once recruited to phosphorylated Rad9, Rad53 is positioned near Mec1, enabling Mec1-dependent priming phosphorylation of Rad53[34]. Oligomerized Rad9 then acts as a scaffold, clustering Rad53 molecules to

[1]Dipartimento di Biotecnologie e Bioscienze, Università degli Studi di Milano-Bicocca, Milano, Italy. [2]These authors contributed equally: Erika Casari, Marco Gnugnoli. e-mail: mariapia.longhese@unimib.it

promote in-trans autophosphorylation, thereby generating the fully active kinase, which subsequently dissociates from Rad9[35,36].

Sae2 not only promotes Mre11 endonuclease activity but also attenuates checkpoint signaling. In the absence of Sae2, or in the presence of an endonucleolytically inactive Mre11 variant, Mre11 and Tel1 persist at DNA ends, leading to Tel1 hyperactivation[37–39]. However, unlike *mre11* nuclease-defective cells, *sae2*Δ cells additionally display excessive Rad9 accumulation at DSBs and persistent Rad53 phosphorylation[39–42], indicating that Sae2 inhibits Rad53 activation independently of its role in MRX stimulation.

Sae2/CtIP activity is regulated by phosphorylation from two kinase classes during the cell cycle and following DNA damage. Cyclin-dependent kinase (CDK) phosphorylates S267 in Sae2[43] and T847 in human CtIP[44]. Structural data suggest that phosphorylated S267 forms salt bridges with R187 of Mre11 and R77 of Rad50[26,27], suggesting that it can promote Mre11 endonuclease activity by stabilizing an MRX conformation that allows proper Mre11 positioning on DNA. Accordingly, a *sae2-S267A* mutant, in which S267 cannot be phosphorylated, shows deficient MRX endonuclease activation, whereas the phospho-mimetic *sae2-S267E* mutant is proficient in supporting MRX-mediated cleavage events[18,43,45]. This CDK-mediated phosphorylation is restricted to the S and G2 phases of the cell cycle[43,46], ensuring that HR occurs only after DNA replication has provided a homologous template. However, Sae2^{S267E} activity is partially lost upon λ phosphatase treatment[45], suggesting that S267 phosphorylation is necessary but not sufficient for full activation of MRX endonuclease activity.

Sae2 is also subjected to Mec1 and/or Tel1 phosphorylation at multiple residues in response to DNA damage, including T90 and T279, with T279 equivalent to T859 in human CtIP and T818 in *Xenopus laevis* CtIP[47–49]. Interestingly, synthetic Sae2 peptides phosphorylated at either T90 or T279 have been shown to interact with the Forkhead associated 1 (FHA1) domain of Rad53 in vitro[50]. Furthermore, replacement of both T90 and T279 to alanine leads to hypersensitivity to DNA-damaging agents and Rad53 hyperactivation upon MMS treatment[50,51], suggesting that Mec1/Tel1-mediated phosphorylation supports Sae2 function in checkpoint attenuation.

Here, we investigate how phosphorylation regulates the dual function of Sae2 in suppressing checkpoint activation and promoting MRX-dependent DNA end clipping. By combining mutational analysis with AlphaFold3-based structural modeling, we show that phosphorylation of Sae2 at either T90 or T279 residue by the checkpoint kinases Mec1 and Tel1 is essential to restrain Rad9-Rad53 interaction and for dampening checkpoint activation. Moreover, phosphorylation at Sae2 T279, but not at T90, functions together with CDK-dependent phosphorylation of S267 to promote MRX-dependent processing of DNA ends, thereby supporting recombination. A phosphomimetic Sae2^{T279E} variant partially rescues both the DNA damage sensitivity and the hairpin resolution defects of Tel1-deficient cells, suggesting that Tel1 supports MRX-mediated cleavage events primarily via Sae2 T279 phosphorylation.

Results

Phosphorylation of Sae2 at either T90 or T279 is sufficient to limit Rad9-Rad53 association and Rad53 activation

Both the absence of Sae2 and expression of the nuclease-deficient *mre11-H125N* allele lead to accumulation of Mre11 and Tel1 at DNA ends[38,39]. However, unlike nuclease-inactive *mre11-H125N* cells, *sae2*Δ cells exhibit excessive Rad9 accumulation at DSBs and Rad53 hyperactivation, resulting in persistent cell-cycle arrest[39]. This likely explains the greater DNA damage sensitivity of *sae2*Δ cells relative to *mre11-H125N* cells[38–42,51] and indicates that Sae2 negatively regulates Rad53 activation independently of its role in stimulating MRX endonuclease activity.

Sae2 is phosphorylated in a Mec1- and Tel1-dependent manner at residues T90 and T279[47]. Synthetic Sae2 peptides phosphorylated at either site bind the Rad53 FHA1 domain in vitro[50]. Furthermore, phosphorylated T90 and T279 act redundantly to promote DNA damage resistance and checkpoint shutdown[50,51], suggesting that these phosphorylation events control Sae2-mediated inhibition of Rad53.

Consistent with prior work[50,51], cells expressing a Sae2 variant in which both T90 and T279 are replaced with alanine (*sae2-T90A T279A*) showed sustained Rad53 phosphorylation after treatment with the radiomimetic drug phleomycin and subsequent transfer to medium lacking phleomycin (Fig. 1A). By contrast, persistent Rad53 phosphorylation was not observed in cells carrying either single *sae2-T90A* or *sae2-T279A* mutation (Fig. 1A), indicating that T90 and T279 act redundantly to suppress checkpoint activation. Rad53 phosphorylation decreased with wild-type kinetics in cells expressing a phosphomimetic Sae2 mutant in which both T90 and T279 are replaced with glutamic acid (*sae2-T90E T279E*) (Fig. 1A), underscoring the importance of T90/T279 phosphorylation for checkpoint attenuation. Moreover, *sae2-T90E T279A* and *sae2-T90A T279E* also showed wild-type Rad53 phosphorylation kinetics (Fig. 1A), indicating that phosphorylation at either site is sufficient for Sae2-dependent downregulation of Rad53.

While T279 is conserved across eukaryotes (including human CtIP), T90 is not. Instead, the position equivalent to T90 is occupied by an acidic residue (Supplementary Fig. 1), indicating that a negative charge, rather than threonine per se, is the conserved feature.

The persistent DNA damage-induced Rad53 activation in *sae2-T90A T279A* cells correlates with heightened sensitivity to phleomycin and to camptothecin (CPT), which traps the Top1 covalent intermediate and yields replication-dependent DSBs[52]. Indeed, *sae2-T90A T279A* cells were more sensitive to both CPT and phleomycin than wild type, whereas cells carrying a single T90A or T279A substitution, or the phosphomimetic T90E and/or T279E mutation, were not (Fig. 1B). Although Rad53 phosphorylation in *sae2-T90A T279A* cells resembles that observed in *sae2*Δ cells (Fig. 1A), the CPT and phleomycin sensitivity of the double alanine mutant is milder than that of *sae2*Δ cells (Fig. 1B), consistent with additional Sae2 functions beyond checkpoint downregulation[53]. Notably, *sae2-T90E*, *sae2-T279E*, and *sae2-T90E T279E* cells did not show increased DNA-damage resistance compared to the wild type (Supplementary Fig. 2).

Rad53 activation relies on Rad9: once phosphorylated by Mec1 or Tel1, Rad9 first acts as an adapter to promote Mec1-Rad53 interaction and Mec1-dependent phosphorylation of Rad53, then serves as a scaffold that clusters Rad53 molecules to enable in-trans autophosphorylation and full kinase activation[29–36]. Because Sae2 has been proposed to dampen Rad53 activation by antagonizing Rad9-Rad53 interaction[39,54], we immunoprecipitated Rad9-HA from extracts of undamaged, exponentially growing cells and assessed Rad53 co-purification by immunoblotting. In wild-type and *sae2-T90E T279E* cells, Rad53 bound to Rad9 was below the limit of detection (Fig. 1C). By contrast, *sae2*Δ and *sae2-T90A T279A* cells displayed detectable Rad53 in Rad9 immunoprecipitates together with Rad53 phosphorylation, consistent with Rad53 activation even under unperturbed conditions (Fig. 1C).

Because Rad53 kinase activation requires in-trans autophosphorylation, we measured Rad53 activity using the in situ autophosphorylation (ISA) assay[35]. ISA signal was barely detectable in extracts from undamaged, exponentially growing wild-type and *sae2-T90E T279E* cells, but increased in *sae2*Δ and *sae2-T90A T279A* cells (Fig. 1D), indicating Rad53 activation. Together, these data indicate that phosphorylation of either T90 or T279 is required for Sae2 to restrain Rad53-Rad9 association and, consequently, Rad53 activation.

Evaluation of the Sae2-Rad53 interaction by AlphaFold3 modeling and targeted mutagenesis

To explore the Sae2-Rad53 interface, we generated AlphaFold3 models of Sae2 phosphorylated at T90 and T279 in complex with the Rad53 FHA1 domain (Fig. 2). The models predict contacts between Rad53 R70, as well as the residues S85, N86, and T106 (see Supplementary Fig. 3 for the alignment of *S. cerevisiae* Rad53 FHA1 with homologs from other organisms), with phosphorylated T90 of Sae2 and, to a lesser extent, with phosphorylated T279 (Fig. 2A, B, E). When phosphorylated T90 is absent, as in the Sae2^{T90A} mutant, AlphaFold3 predicts a higher probability of phosphorylated T279 contacting the FHA1 domain (Fig. 2C, D, F), providing a structural rationale for the functional redundancy of the two sites.

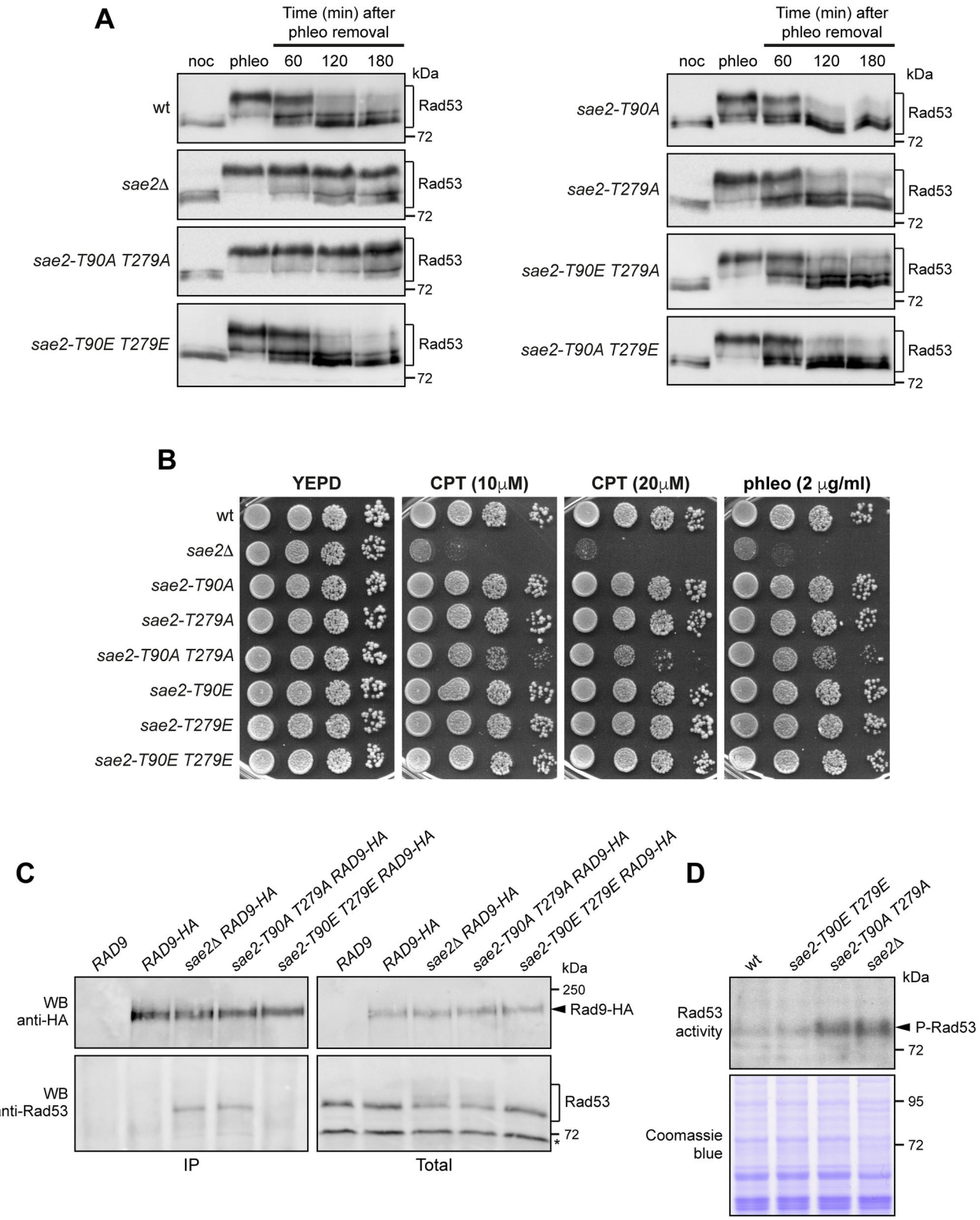

Fig. 1 | Phosphorylated Sae2 T90 and T279 act redundantly to downregulate Rad53 and support DNA damage resistance. A Phleomycin (30 μg/mL) was added to nocodazole-arrested (noc) cells. After 2 h in the presence of phleomycin (phleo), cells were transferred to medium lacking both phleomycin and nocodazole. Aliquots collected at the indicated times after phleomycin removal were analyzed by Western blot with an anti-Rad53 antibody. This experiment was performed independently three times with similar results. **B** Drug-sensitivity assay. Exponentially growing cultures were serially diluted (1:10) and spotted on yeast extract, bactopeptone, and glucose (YEPD) plates with or without CPT or phleomycin. **C** Co-immunoprecipitation. Protein extracts from exponentially growing cells were analyzed by Western blotting with anti-HA (Rad9-HA) and anti-Rad53 antibodies either directly (total) or after immunoprecipitation (IP) of Rad9-HA with an anti-HA antibody. * indicates a cross-hybridization band. This experiment was performed independently three times with similar results. **D** In situ autophosphorylation (ISA) assay of protein extracts from exponentially growing cells. Equal loading was verified by Coomassie blue staining of the same extracts. This experiment was performed independently two times with similar results.

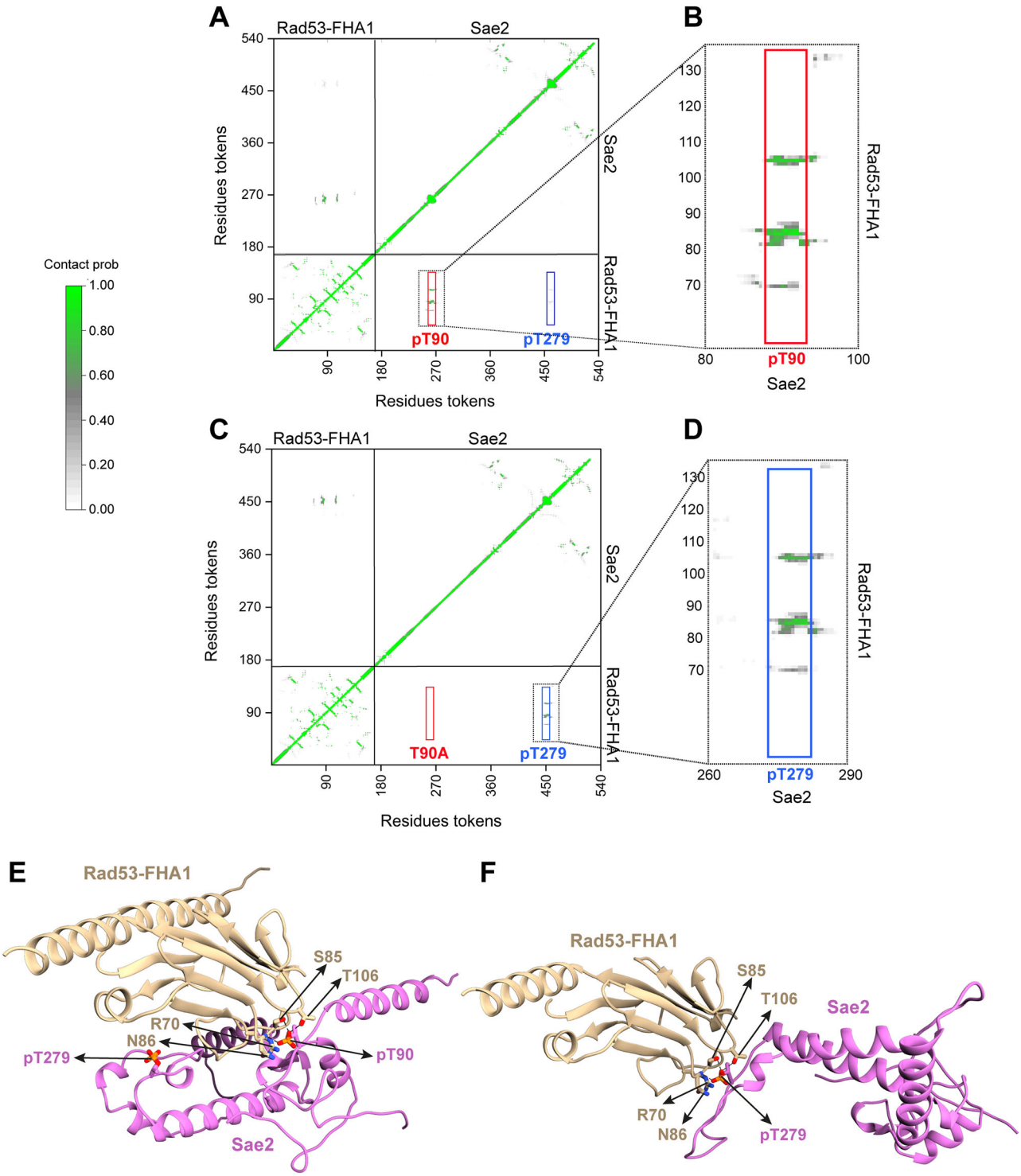

Fig. 2 | AlphaFold3-based model of Sae2 phosphorylated on T90 and T279 bound to Rad53 FHA1 domain. A Inter-chain contact probability map predicted by AlphaFold3 for wild-type Sae2 phosphorylated at T90 and T279 bound to Rad53-FHA1. Axes list residue tokens in sequence order for Rad53 and Sae2. Because post-translational modifications are encoded by multiple tokens, phosphorylated sites appear as expanded blocks; rectangles mark token groups for pT90 (red) and pT279 (blue). **B** Zoom of the highest probability contact from (**A**), involving Sae2 residues 80–100 and Rad53 residues 70–135 around pT90. **C** Contact probability map as in (**A**) but with Sae2-T90A phosphorylated only at T279. The pT90 block is absent; the rectangle highlights pT279 (blue). **D** Zoom of the highest probability contact from (**C**), centered on pT279, involving Sae2 residues 260–290 and Rad53 residues 70–135. **E** Confident portions of the model shown as cartoons for the complexes in (**A**). **F** Confident portions of the model shown as cartoons for the complexes in (**C**). Interfacial side chains are shown as sticks; phosphorylated residues (pT90, pT279) are shown as spheres.

Because the R70A substitution disrupts the conserved phospho-ligand recognition of FHA1 and abolishes binding of Rad53 FHA1 to peptides containing phosphorylated T90 and T279[50], we tested the interface in vivo by substituting Sae2 T90 and T279 with positively charged residues (T90R and T279R) and by introducing the charge-reversal R70E mutation in Rad53.

Like *sae2*Δ, *sae2-T90R T279R* cells exhibited persistent Rad53 phosphorylation after phleomycin removal, whereas *rad53-R70E* cells did not (Fig. 3A), suggesting that R70E alone does not impair Sae2-dependent regulation, likely because other basic residues in FHA1 (e.g., R83, K87) can stabilize binding to phosphorylated Sae2. The *rad53-R70E* allele also had no effect on Rad53 phosphorylation (Fig. 3A) or DNA damage sensitivity of *sae2*Δ cells (Fig. 3B). The presence of the *rad53-R70E* allele into *sae2-T90R T279R* cells suppressed Rad53 hyperactivation and DNA damage sensitivity. In fact, Rad53 phosphorylation decreased with wild-type kinetics in *rad53-R70E sae2-T90R T279R* cells (Fig. 3A), which also showed reduced CPT and phleomycin sensitivity relative to *sae2-T90R T279R* cells (Fig. 3B). By contrast, *rad53-R70E* neither reduced Rad53 phosphorylation (Fig. 3A) nor alleviated DNA damage sensitivity (Fig. 3B) of *sae2-T90A T279A* cells, where T90 and T279 cannot be phosphorylated and thus cannot provide the negative charges required to interact with Rad53. These findings support a phosphorylation-dependent electrostatic interaction-based mechanism at the Rad53-Sae2 interface in which negative charge supplied by phosphorylation (T90/T279) is required for Rad53 interaction and inhibition.

The *rad53-R70E* allele also restored the ability of *sae2-T90R T279R* cells to restrain Rad9-Rad53 interaction. In fact, when Rad9-HA was immunoprecipitated from undamaged, exponentially growing cells, Rad53 failed to co-immunoprecipitate with Rad9 in *rad53-R70E sae2-T90R T279R* immunoprecipitates, whereas it was detected (together with Rad53 phosphorylation) in *sae2-T90R T279R* cells (Fig. 3C).

Phosphorylation of Sae2 at both T279 and S267 is required to promote Mre11 cleavage events

In both yeast and mammals, Sae2/CtIP stimulates Mre11 activity within the MRX complex[18]. This function is mediated by a direct Sae2-Rad50 interaction that requires CDK-dependent phosphorylation of Sae2 S267, enabling the formation of salt bridges with Mre11 R187 and Rad50 R77[18,26,27]. However, although the phosphomimetic Sae2-S267E mutant supports MRX-dependent DNA cleavage, its activity is partially lost upon λ phosphatase treatment[45], suggesting that S267 phosphorylation is necessary but not sufficient for full activation of MRX endonuclease activity.

Our AlphaFold3-based analysis suggested that concomitant phosphorylation at S267 and T279 promotes an Mre11 conformation resembling the active, DNA-cleaving state[26]. In particular, phosphorylated T279 is predicted to contact Rad50 K6, a residue affected by *rad50-s* mutations that impair Sae2-Rad50 interactions (Supplementary Fig. 4)[26]. To evaluate the functional interplay between S267 and T279 in supporting Mre11 cleavage activity, we tested phospho-site mutants for defects in hairpin resolution and meiotic recombination. Hairpin cleavage was assessed using a genetic assay developed by Lobachev et al., in which inverted Alu elements inserted into the *LYS2* gene on chromosome II stimulate ectopic recombination with a truncated *lys2-Δ5′* on chromosome III, generating Lys$^+$ recombinants (Fig. 4A)[16]. This recombination event requires both Mre11 endonuclease activity and Sae2, which process hairpin-capped DSBs formed from extrusion of the inverted Alu sequences[16].

We previously showed that substitution of T279 with a non-phosphorylatable alanine (*sae2-T279A*) residue reduced the frequency of Lys$^+$ recombinants compared to wild type, whereas the phosphomimetic *sae2-T279E* did not[26] (Fig. 4B). To define the relative contributions of S267 and T279 phosphorylation, we analyzed single and double alanine mutants. Consistent with previous results[51], *sae2-S267A* cells showed a strong reduction in Lys$^+$ recombinants (Fig. 4B). However, the defect was less severe than that observed in *sae2*Δ cells (Fig. 4B), indicating that Sae2^{S267A} retains residual function. By contrast, *sae2-S267E*, *sae2-T279E*, and *sae2-S267E T279E* showed no recombination defects (Fig. 4B). Strikingly, when both S267 and T279 were mutated to alanine, recombination dropped to the level observed in *sae2*Δ and in nuclease-defective *mre11-H125N* cells (Fig. 4B), indicating that both residues are required to fully support MRX cleavage activity. In contrast, T90 does not appear to contribute, as *sae2-T90A* cells showed no reduction in Lys$^+$ recombination and the T90A mutation did not exacerbate the recombination defects of *sae2-T279A* or *sae2-S267A* cells (Fig. 4B).

During meiosis, the topoisomerase-like protein Spo11 initiates recombination by cleaving DNA strands and remains covalently bound to 5′ DNA ends[55]. Removal of Spo11 attached to short oligonucleotides, catalyzed by Mre11 and Sae2, is essential for subsequent homologous recombination steps[4,56]. Consistent with previous studies[43,57], no viable spores were detected in *sae2*Δ diploids, whereas *sae2-S267A* diploids retained approximately 10% spore viability (Fig. 4C). *sae2-T279A* diploids showed wild-type spore viability, but combining S267A and T279A mutations further reduced spore viability compared to S267A alone (Fig. 4C), indicating a role for T279 phosphorylation in Spo11 removal. Consistent with no role of T90 phosphorylation in promoting Mre11 cleavage events, the T90A mutation did not reduce spore viability and did not worsen the sporulation defects of *sae2-T279A* and *sae2-S267A* cells (Fig. 4C).

Cells carrying the nuclease-defective *mre11-H125N* allele were more sensitive to CPT and phleomycin than *sae2-S267A* cells (Fig. 4D)[39]. If phosphorylation of both Sae2 S267 and T279 is primarily involved in the activation of Mre11 endonuclease, *sae2-S267A T279A* and *mre11-H125N* cells should show similar DNA damage sensitivity. Indeed, although *sae2-T279A* did not show obvious DNA damage sensitivity, *sae2-S267A T279A* cells displayed CPT and phleomycin sensitivity greater than *sae2-S267A* cells and comparable to *mre11-H125N* cells (Fig. 4D). By contrast, introducing the T90A mutation did not increase the DNA damage sensitivity of *sae2-S267A* cells (Fig. 4D).

To further probe the relative contribution of S267 and T279 phosphorylation, we introduced the phosphomimetic S267E and T279E mutations into the reciprocal alanine background. Although the *sae2-S267E*, *sae2-T279E*, and *sae2-S267E T279E* alleles supported recombination, spore viability, and DNA-damage resistance in an otherwise wild-type background (Fig. 4B–D), introducing S267E into *sae2-T279A* cells or T279E into *sae2-S267A* decreased recombination (Fig. 4B), spore viability (Fig. 4C), and DNA-damage resistance (Fig. 4E) compared with the respective single-alanine mutants. Thus, phosphomimicry at one site does not rescue when the other site cannot be phosphorylated, indicating that phosphorylation of both S267 and T279 is required for full Sae2 function in promoting Mre11-dependent cleavage.

Loss of Sae2 S267 and T279 phosphorylation does not increase Rad9 binding at DSBs or Rad53 activation

Unlike nuclease-defective *mre11-H125N* cells, deletion of *SAE2* increases Rad9 association with DSBs. Elevated Rad9 at DSBs hyperactivates the Rad53 checkpoint kinase[37,38] and acts as a barrier to Sgs1-Dna2-mediated resection[39–42], while Rad53 hyperactivation inhibits Exo1 via phosphorylation[58].

If concurrent phosphorylation of Sae2 at S267 and T279 primarily stimulates Mre11 endonuclease activity, then *sae2-S267A T279A* cells should display Rad9 association with DSBs comparable to wild type. To test this, we used ChIP-qPCR to examine Rad9 binding at an endonuclease-induced DSB by introducing *sae2-S267A*, *sae2-T279A*, and *sae2-S267A T279A* alleles into the JKM139 strain, which expresses the endonuclease HO under a *GAL* promoter. Galactose addition induces HO, which generates a single DSB at the *MAT* locus that cannot be repaired by HR because the homologous donor loci *HML* and *HMR* are deleted. As observed for *mre11-H125N*, Rad9 binding at the HO-induced DSB in *sae2-S267A*, *sae2-T279A*, and *sae2-S267A T279A* cells was similar to wild type, whereas only *sae2*Δ cells showed elevated Rad9 accumulation (Fig. 5A). Protein abundance was comparable across strains (Fig. 5B). Thus, loss of S267 and T279 phosphorylation does not impair the ability of Sae2 to limit Rad9 association at DSBs.

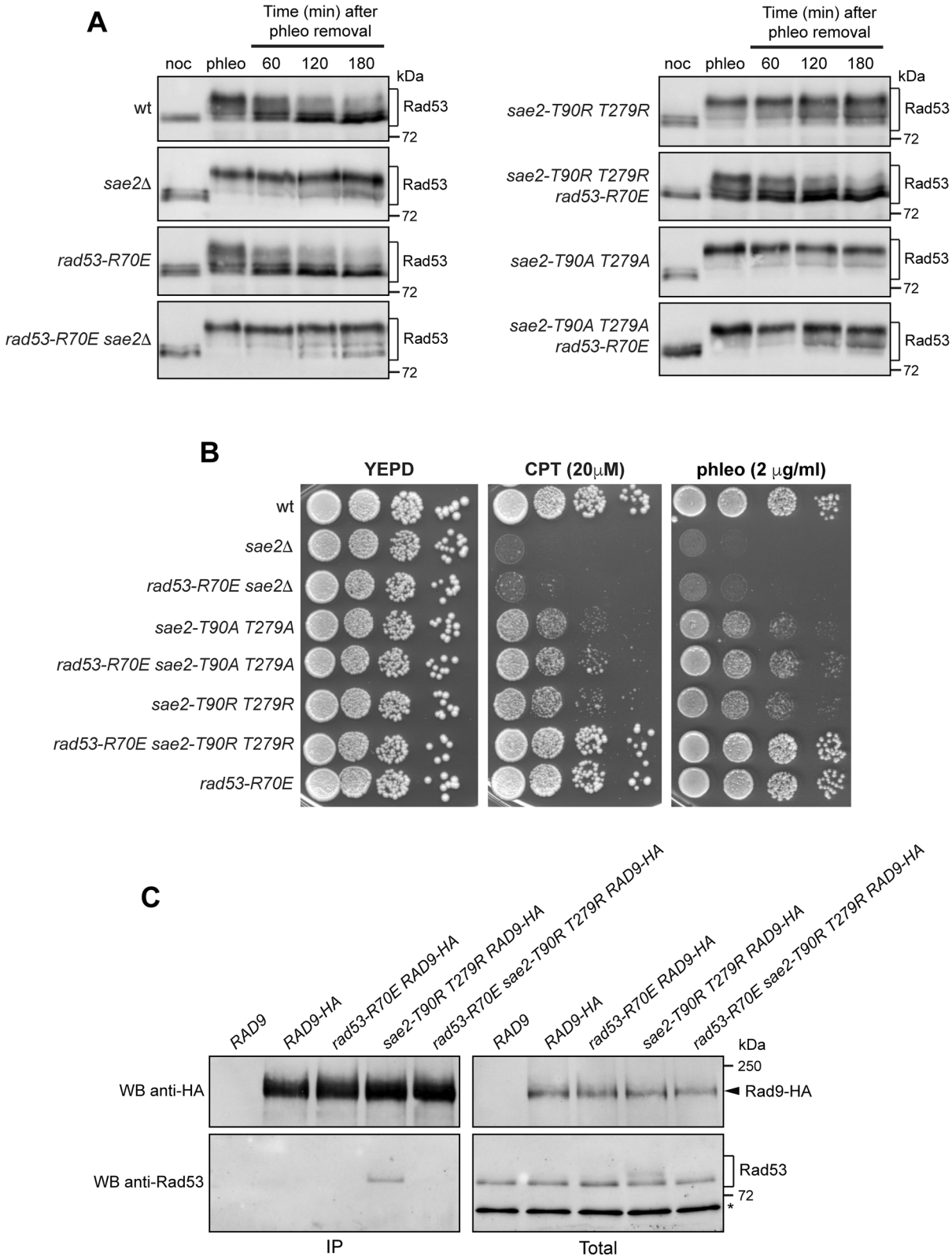

Fig. 3 | Charge reversal mutations between Sae2 T90/T279 and Rad53 R70. **A** Phleomycin (30 μg/mL) was added to nocodazole-arrested (noc) cells. After 2 h in the presence of phleomycin (phleo), cells were transferred to medium lacking both phleomycin and nocodazole. Aliquots collected at the indicated times after phleomycin removal were analyzed by Western blot with an anti-Rad53 antibody. This experiment was performed independently three times with similar results. **B** Drug-sensitivity assay. Exponentially growing cultures were serially diluted (1:10) and spotted on YEPD plates with or without CPT or phleomycin. **C** Co-immunoprecipitation. Protein extracts from exponentially growing cells were analyzed by Western blotting with anti-HA (Rad9-HA) and anti-Rad53 antibodies either directly (total) or after IP of Rad9-HA with an anti-HA antibody. * indicates a cross-hybridization band. This experiment was performed independently three times with similar results.

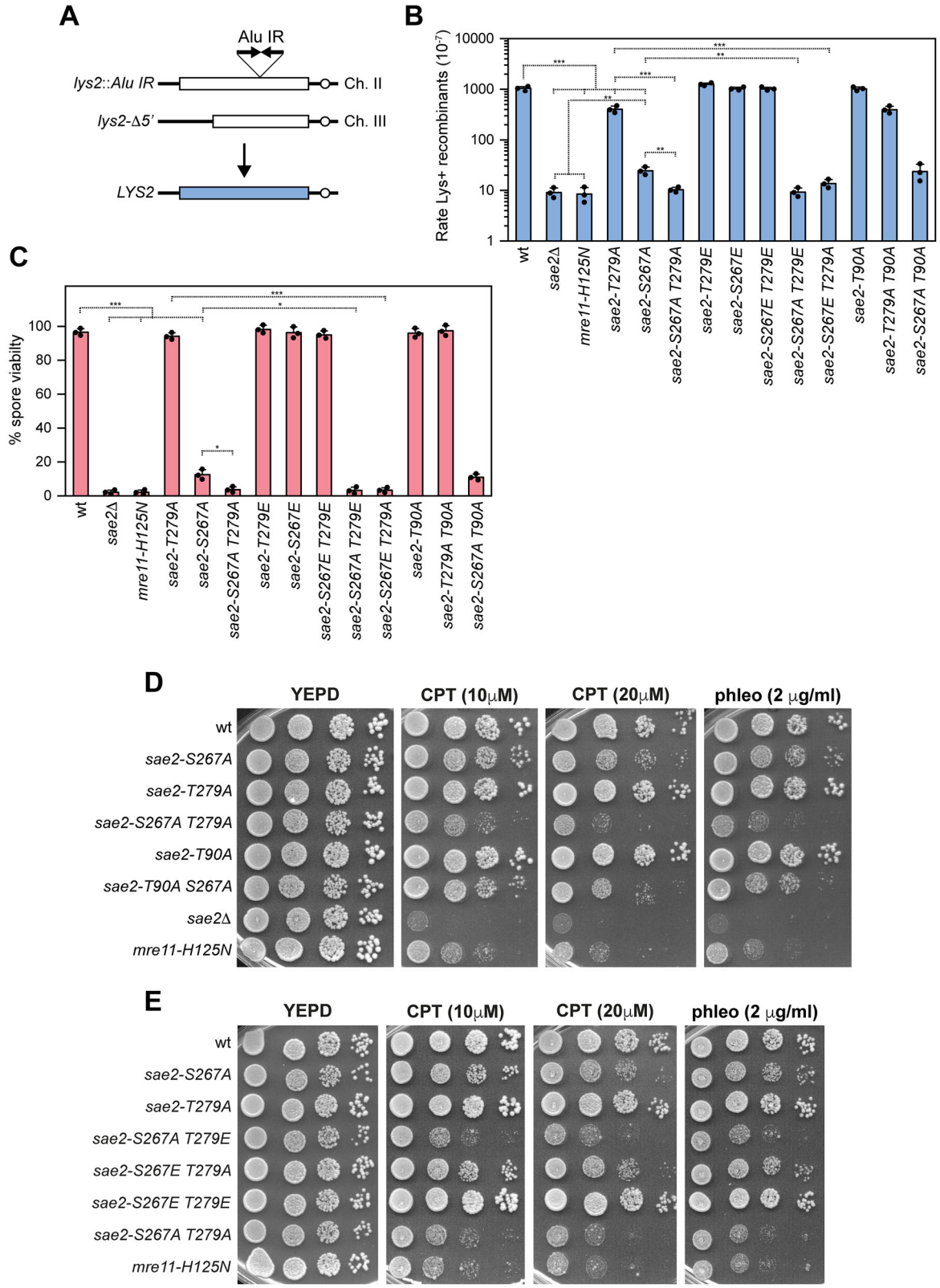

Fig. 4 | Phosphorylated Sae2 S267 acts with T279 to promote MRX-dependent cleavage. A Schematic representation of the *lys2::Alu IR* and *lys2-Δ5′* ectopic recombination system. **B** Recombination frequency in strains carrying the *lys2::Alu IR* and *lys2-Δ5′* ectopic recombination system. Rate of Lys^+ recombinants were derived from the median recombination frequency. Mean of three independent experiments are represented with error bars denoting s.d. $^{***}p < 0.005$, $^{**}p < 0.001$ (unpaired two-tailed Student's *t* test). See Supplementary Data for statistical analysis. **C** Sporulation efficiency. Diploids homozygous for the indicated alleles were induced to enter meiosis. Mean of three independent experiments are represented with error bars denoting s.d. $^{***}p < 0.005$, $^{*}p < 0.05$ (unpaired two-tailed Student's *t* test). See Supplementary Data for statistical analysis. **D, E** Drug-sensitivity assay. Exponentially growing cultures were serially diluted and spotted on YEPD plates with or without CPT or phleomycin.

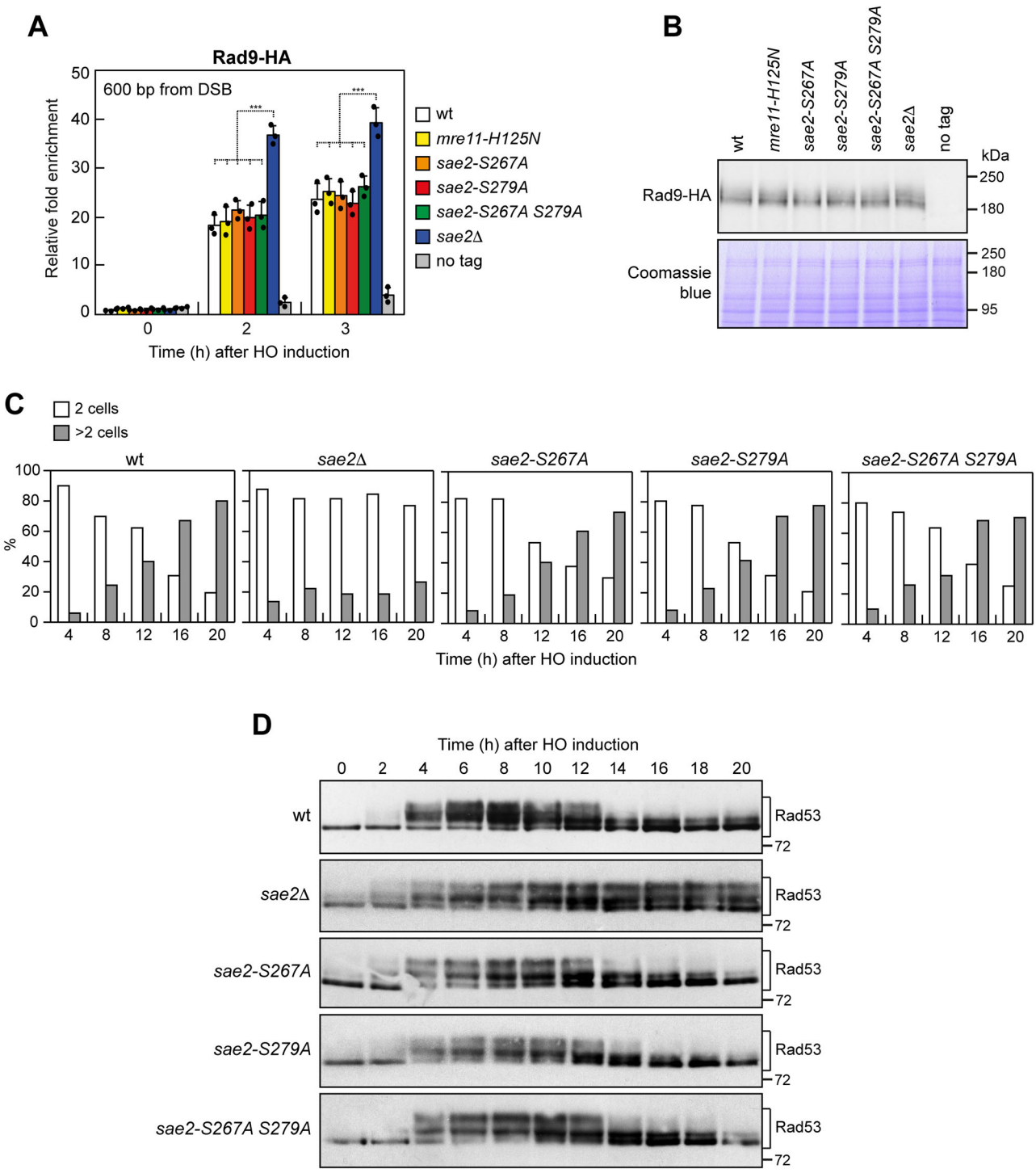

Fig. 5 | S267/T279 phosphorylation of Sae2 does not increase Rad9 binding at DSBs or sustain Rad53 activation. A ChIP and qPCR. Exponentially growing YEPR cell cultures were shifted to YEPRG to induce HO expression, followed by ChIP analysis of Rad9-HA at 600 bp from the HO-cut site. In all diagrams, ChIP signals were normalized to the corresponding input signal at each time point. Mean of three independent experiments are represented with error bars denoting s.d. ***$p < 0.005$ (unpaired two-tailed Student's t test). See Supplementary Data for statistical analysis. **B** Western blot analysis with an anti-HA antibody of protein extracts from exponentially growing cells. Equal loading was verified by Coomassie blue staining of the same extracts. This experiment was performed independently three times with similar results. **C** Adaptation assay. YEPR G1-arrested cell cultures were plated on galactose-containing plates (time zero). At the indicated times, 200 cells for each strain were scored to determine two-cell dumbbells (2 cells) and microcolonies with >2 cells. This experiment was performed independently two times with similar results. **D** Checkpoint kinetics. Exponentially growing YEPR cell cultures were shifted to YEPRG at time zero to induce HO. Western blot analysis of protein extracts was performed with an anti-Rad53 antibody. This experiment was performed independently two times with similar results.

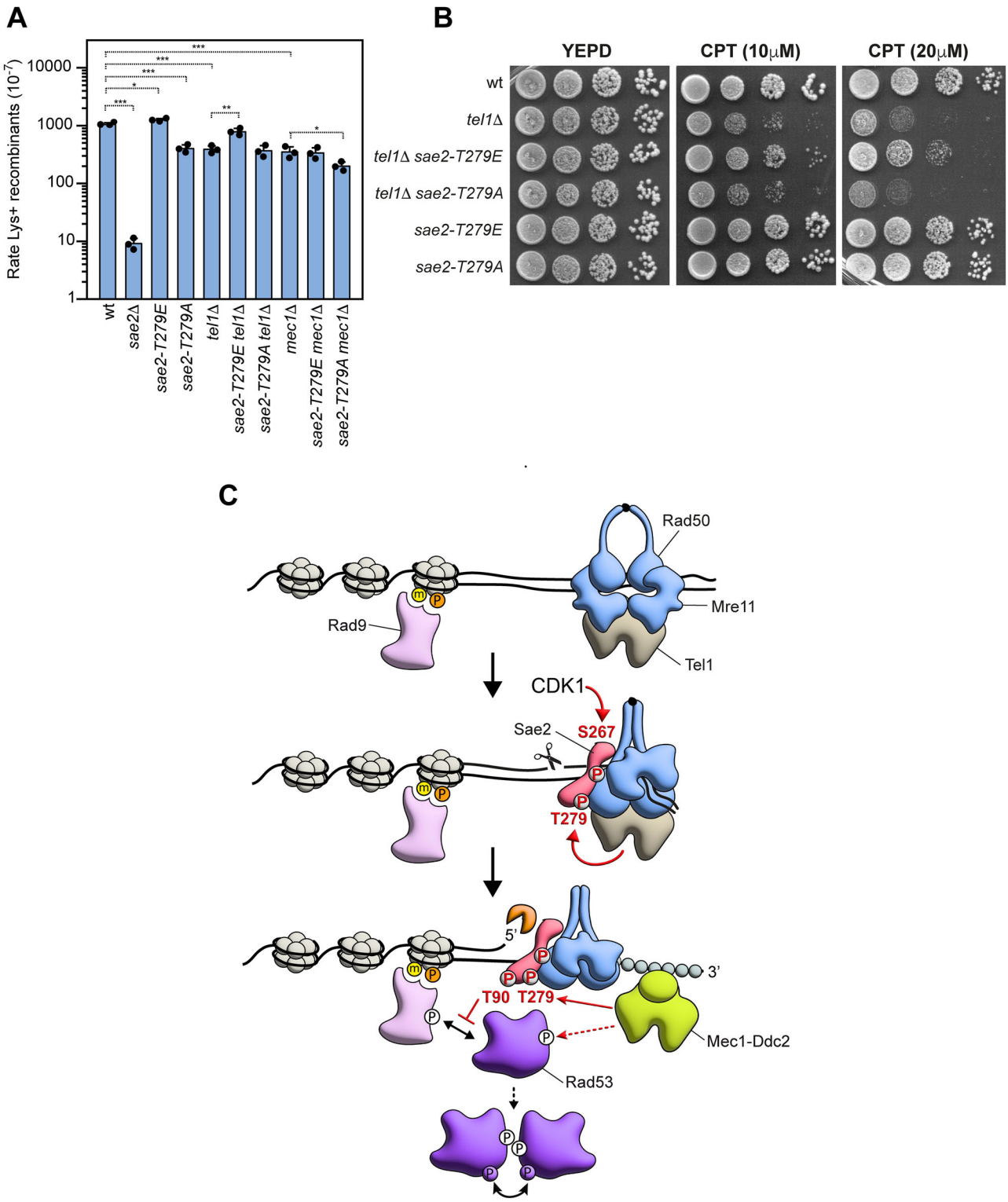

Because increased Rad9 association with DSBs in *sae2*Δ cells leads to Rad53 hyperactivation, *sae2-S267A*, *sae2-T279A*, and *sae2-S267A T279A* cells should exhibit a wild-type checkpoint response. Cells harboring a single irreparable DSB typically undergo checkpoint-mediated cell-cycle arrest and subsequently decrease Rad53 activation to resume the cell cycle through a process called adaptation[59,60]. The increased Rad9 association with DSBs in *sae2*Δ cells leads to Rad53 hyperactivation that prevents cells from adapting to a single irreparable DSB[37,38]. We therefore analyzed the checkpoint response of *sae2-S267A*, *sae2-T279A*, and *sae2-S267A T279A* cells to an irreparable HO-induced DSB. When plated on galactose to induce HO, all cell cultures arrested as two-cell dumbbells (Fig. 5C). Thereafter, while most *sae2*Δ cells remained arrested after 20 h, wild-type, *sae2-S267A*, *sae2-T279A*, and *sae2-S267A T279A* cells formed microcolonies (>2 cells) after ~12 h (Fig. 5C). Similarly, upon galactose addition to exponentially growing cells, Rad53 phosphorylation persisted for at least 20 h in *sae2*Δ but began to decline after ~12 h in wild-type, *sae2-S267A*, *sae2-T279A*, and *sae2-S267A T279A* cells (Fig. 5D). Thus, loss of Sae2 S267/T279 phosphorylation does not impair the ability of Sae2 to restrain Rad53 activation.

Fig. 6 | Effect of T279E mutation on hairpin resolution and DNA damage sensitivity of cells lacking Mec1 or Tel1. A Recombination frequency of strains with the *lys2::Alu IR* and *lys2-Δ5′* ectopic recombination system. Rates of Lys^+ recombinants were derived from the median recombination frequency. Mean of three independent experiments are represented with error bars denoting s.d. $^{***}p < 0.005$, $^{**}p < 0.001$, $^{*}p < 0.05$ (unpaired two-tailed Student's *t* test). See Supplementary Data for statistical analysis. Cells carrying the deletion of *MEC1* also contain the deletion of *SML1*. **B** Exponentially growing cultures were serially diluted and spotted on YEPD plates with or without CPT. **C** Working model. The MRX complex is rapidly recruited to DNA ends, where it loads and activates Tel1. Rad9 binds chromatin via methylated histone H3 (yellow m-labeled circle) and phosphorylated histone H2A (orange P-labeled circle). ATP hydrolysis in Rad50 drives a conformational change in which the Rad50 coiled coils zip up, and the Mre11 dimer rotates relative to the Rad50 heads. CDK and Tel1/Mec1 phosphorylate Sae2 on S267 and T279, respectively, promoting Sae2-Rad50 binding; this interaction stabilizes an ADP-bound Mre11-Rad50 state that is competent for DNA cleavage. MRX-Sae2 initiates resection by nicking the 5′-terminated strand. Exo1 and Dna2-Sgs1 extend resection to generate ssDNA, which is coated by RPA and recruits Mec1-Ddc2. Mec1 then phosphorylates Rad9, creating docking sites for Rad53 and enabling Mec1-dependent Rad53 priming phosphorylation. Phosphorylated Rad9 clusters Rad53 to promote in-trans autophosphorylation (purple dots) and full kinase activation. In parallel, Mec1/Tel1 phosphorylation of Sae2 at T90 and/or T279 creates a FHA1-binding site for Rad53; Sae2-Rad53 engagement competes with Rad9 for Rad53 FHA1, thereby limiting Mec1-dependent Rad53 phosphorylation (dashed line) and Rad53 in-trans autophosphorylation (dashed line) and enabling checkpoint shutdown.

Sae2 T279E substitution partially bypasses the requirement of Tel1 in DNA damage resistance and hairpin resolution

T279 is among the Sae2 residues phosphorylated in a Mec1/Tel1-dependent manner[47], suggesting that the checkpoint can control MRX cleavage activity. Consistent with this hypothesis, simultaneous deletion of *TEL1* and *MEC1* (kept viable by *SML1* deletion) almost completely abolishes meiotic DSB processing[61]. Furthermore, cells lacking *MEC1* (again kept viable by *SML1* deletion) or *TEL1* showed reduced Lys^+ recombinants compared to wild-type cells (Fig. 6A).

If the defect in hairpin cleavage of *mec1*Δ and/or *tel1*Δ cells is primarily due to impaired T279 phosphorylation, it should be suppressed by a phosphomimetic *sae2-T279E* allele. Indeed, *tel1*Δ *sae2-T279E* double mutant cells showed increased Lys^+ recombinants (Fig. 6A) and improved CPT resistance (Fig. 6B) compared to *tel1*Δ alone, indicating partial rescue of the defect. Moreover, introducing the non-phosphorylatable *sae2-T279A* allele into *tel1*Δ cells did not further exacerbate the recombination defect (Fig. 6A) or CPT hypersensitivity (Fig. 6B), suggesting that Tel1 and phosphorylated T279 act in the same pathway. In contrast, the phosphomimetic *sae2-T279E* allele did not suppress the recombination defect of *mec1*Δ cells (Fig. 6B), and introducing the non-phosphorylatable *sae2-T279A* allele into *mec1*Δ cells further reduced the rate of Lys^+ recombinants (Fig. 6B). These results suggest that Mec1 contributes to hairpin resolution through additional targets beyond Sae2 T279.

Discussion

Sae2 fulfills at least two distinct functions at DNA DSBs: it dampens activation of the checkpoint kinase Rad53, and it promotes DNA end clipping by the MRX complex. The ability of Sae2 to inhibit Rad53 activation is independent of its role in stimulating MRX nuclease activity. Here, we provide mechanistic insights into how Sae2 integrates phosphorylation inputs from CDK and from the checkpoint kinases Mec1 and Tel1 to coordinate these two functions.

Our AlphaFold3-based modeling predicts a phosphorylation-dependent interaction between Sae2 T90/T279 and the Rad53 FHA1 domain, with T90 showing the higher binding probability. The sequence contexts around these sites resemble, but are not identical to, the TXAD consensus for FHA1 specificity identified by phosphopeptide-binding studies[62]. Specifically, T90 lies within TQFD and T279 within TQEG, with the T279 context more divergent from the optimal motif, suggesting a predominant contribution of phosphorylated T90 in making contact with Rad53 FHA1. Nevertheless, when T90 is mutated into alanine, phosphorylated T279 can still support Rad53 binding, allowing control of Rad53 activation.

Functionally, these two sites act redundantly to restrain Rad53 activity. Only the double alanine mutant (*sae2-T90A T279A*) causes persistent Rad53 phosphorylation and hypersensitivity to DNA damage, whereas phosphomimetic substitutions restore wild-type Rad53 inactivation kinetics. AlphaFold3 predictions, together with charge-reversal mutagenesis, support a phosphorylation-dependent electrostatic mechanism in which negative charges on Sae2 (at pT90 and/or pT279) engage interaction with Rad53 R70 to inhibit Rad53 activation. Notably, whereas T279 is conserved across eukaryotes, the position equivalent to T90 is typically occupied by an acidic residue, indicating that a local negative charge, rather than threonine per se, is the conserved feature.

Rad53 activation relies on Rad9 that, once phosphorylated by Mec1 or Tel1, first acts as an adapter to promote Mec1-Rad53 association and Mec1-dependent phosphorylation of Rad53, and then functions as a scaffold to juxtapose Rad53 molecules for in-trans autophosphorylation and full activation[29–36]. We found that loss of phosphorylation at both T90 and T279 increases Rad9-Rad53 assembly and Rad53 in-trans autophosphorylation, supporting a model in which phosphorylated Sae2 at T90 or T279 competes with Rad9 for FHA1 binding, thereby limiting Rad53 activation (Fig. 6C). Because T90/T279 phosphorylation depends on Mec1/Tel1, this mechanism creates a self-limiting circuit in which the checkpoint kinases that initiate checkpoint signaling also promote its resolution by enabling Sae2-mediated inhibition of Rad53, ensuring timely recovery from DNA damage.

Unlike T90, T279 phosphorylation also acts together with CDK-dependent S267 phosphorylation to promote MRX-dependent cleavage events (Fig. 6C). While Sae2 T279A mutation alone has limited effects on hairpin resolution, spore viability, and DNA damage sensitivity, the combined S267A and T279A mutations phenocopy the defects in hairpin resolution and meiotic recombination observed in an *mre11* nuclease-dead mutant. By contrast, the phosphomimetic *sae2-S267E*, *sae2-T279E*, and *sae2-S267E T279E* alleles support recombination, spore viability, and DNA-damage resistance in otherwise wild-type cells. Interestingly, phosphomimicry at one site does not compensate when the other cannot be phosphorylated, underscoring the need for dual phosphorylation to fully activate Mre11 endonuclease.

Consistent with a Mec1/Tel1 role in supporting MRX cleavage via Sae2 T279 phosphorylation, simultaneous loss of *MEC1* and *TEL1* severely impairs meiotic DSB processing[61], whereas single deletions reduce hairpin resolution efficiency. In mammals, CtIP phosphorylation at T847 (yeast S267 equivalent in humans) and T859 (yeast T279 equivalent in humans) has been implicated in DSB resection and Spo11 removal during meiosis[46,49,63,64].

The joint requirement for CDK- and checkpoint-dependent phosphorylation underscores the temporal and spatial control of DNA end resection. CDK-mediated S267 phosphorylation biases MRX activation and resection to S/G2 phases, when a sister chromatid is available as a template. The additional need for Tel1/Mec1-mediated T279 phosphorylation adds a layer of control that restricts resection to DNA damage contexts, preventing unscheduled processing and limiting genomic instability.

Finally, expression of a phosphomimetic T279E variant in *tel1*Δ cells partially restores hairpin resolution and CPT resistance, indicating that Tel1 promotes MRX function primarily through Sae2 T279 phosphorylation. Because CPT traps Top1 on DNA, impeding replication-fork progression[52] and generating DSBs that require resection for homologous recombination, suppression of *tel1*Δ CPT sensitivity by Sae2-T279E indicates that Tel1 contributes to CPT resistance, at least in part, by enabling MRX-mediated resection via Sae2 phosphorylation.

In conclusion, Sae2 integrates phosphorylation inputs from CDK and checkpoint kinases to coordinate DNA end resection and checkpoint activation. This dual control helps balance efficient repair with timely checkpoint shutdown, preventing aberrant DNA processing and safeguarding genome stability.

Methods

Yeast strains and media

Saccharomyces cerevisiae was used as the experimental model. Strain genotypes are listed in Supplementary Table 1. Strain HS21, used to detect hairpin opening, was kindly provided by M.A. Resnick (National Institutes of Health, NC). Strain JKM139, used to detect Rad9 association at the HO-induced DSB and checkpoint adaptation, was kindly provided by J. Haber (Brandeis University, Waltham, USA). Cells were grown in YEP medium (1% yeast extract, 2% bactopeptone) supplemented with 2% glucose (YEPD), 2% raffinose (YEPR) or 2% raffinose and 3% galactose (YEPRG). Gene disruptions and site-specific mutagenesis were generated by one-step PCR-mediated methods. Primers for site-specific mutagenesis are listed in Supplementary Table 2. All experiments were performed at 26 °C.

Western blotting

Protein extracts were prepared by trichloroacetic acid (TCA) precipitation, as described[65]. Frozen cell pellets were resuspended in 100 µL 20% TCA, mixed with acid-washed glass beads, and vortexed for 10 min. Beads were washed with 400 µL of 5% TCA, and the extract collected in a new tube. Proteins were precipitated by centrifugation at 850 × *g* for 10 min, the TCA was removed, and pellets were resuspended in 70 µL 2X Laemmli buffer (60 mM Tris-HCl pH 6.8, 2% SDS, 10% glycerol, 100 mM DTT, 0.2% bromophenol blue), then neutralized with 30 µL 1 M Tris base. Samples were boiled, clarified, and supernatants resolved on 10% SDS-PAGE. Rad53 was detected with an anti-Rad53 polyclonal antibody (Abcam ab104232, 1:2000). HA-tagged proteins were detected by using an in-house anti-HA (12CA5) (1:2000) antibody. Images were acquired with ChemiDoc (Bio-Rad) and analyzed using Image Lab.

Drug sensitivity assay

Overnight saturated cultures were serially diluted 10-fold in water; 5 µl of each dilution were spotted on the indicated plates. Images were taken after 3 days at 26 °C. Each experiment was repeated at least twice.

Hairpin opening assay

HS21 isogenic strains were grown overnight in YEPD. Cultures were counted, and 10^7 cells were plated onto synthetic medium lacking lysine; 500 cells were plated onto complete synthetic medium. Plates were incubated at 26 °C for 3 days and colonies counted. The rate of Lys^+ recombinants was derived from the median recombination frequency across 10 independent isolates per strain, as described[17]. Three independent trials were performed, and the mean recombination rate was calculated.

Bioinformatics

A first model was generated by AlphaFold3 predictors based on the sequence of Sae2, modified with phosphorylation on residues T90 and T279, and the FHA1 domain of Rad53 (aa 1–168). The top-scoring model issued a pTM score of 0.37 and an ipTM score of 0.71. The quality assessment of this model is shown in Supplementary Fig. 5. A second model was generated by AlphaFold3 predictors based on the sequence of $Sae2^{T90A}$, modified with phosphorylation on T279, and the FHA1 domain of Rad53 (aa 1–168), with the top-scoring model giving a pTM score of 0.41 and an ipTM score of 0.57. The quality assessment of these models is shown in Supplementary Fig. 5. Multiple sequence alignment of FHA domains was obtained by Clustal Omega, a program that uses seeded guide trees and HMM profile-profile techniques to generate alignments between three or more sequences available on the EMBL-EBI platform[66]. In detail, the FHA domains from the following sequences from the GenPept database were submitted to Clustal Omega: human Chk2 (accession 1GXC_A), *Drosophila melanogaster* Chk2 (accession BAA28755), *Amphimedon queenslandica* Chk2-like protein (accession XP_019858435), *Centruroides sculpturatus* Chk2-like isoform X2 (accession XP_023214969), *Trichoplax sp. H2* Chk2 (accession RDD46461), *Ciona intestinalis* myosin light chain kinase A (accession XP_002130190), *Caenorhabditis elegans* Chk2 (accession Q9U1Y5), *Armadillidium vulgare* Chk2 (accession RXG73588), *Saccharomyces cerevisiae* Rad53 (accession P22216), *Schizosaccharomyces pombe* Rad53/cds1 (accession Q09170). For Sae2 homologs alignment, the following full sequences were submitted to Clustal Omega: human CTIP (accession Q99708), *Xenopus laevis* CTIP (accession Q6GNV6), *Danio rerio* CTIP (F1R983), *Saccharomyces cerevisiae* Sae2 (P46946), and *Schizosaccharomyces pombe* Ctp1 (O74986).

Chromatin immunoprecipitation and qPCR

Exponentially growing YEPR cultures of JKM139 derivative strains carrying the HO cut site at the *MAT* locus were transferred to YEPRG at time zero. Crosslinking was performed with 1% formaldehyde for 10 min. The reaction was stopped by adding 0.125 M glycine for 5 min. Immunoprecipitation was performed by incubating samples with Dynabeads Protein G (ThermoFisher Scientific) for 3 h at 4 °C in the presence of 5 µg anti-HA (12CA5) antibody. qPCR was performed on a Bio-Rad CFX Connect™ Real-Time System Apparatus. Triplicate samples in 20 µl reaction mixture containing 10 ng of template DNA, 300 nM primers, 2X SsoFast™ EvaGreen supermix (Bio-Rad #1725201) (2X reaction buffer with dNTPs, Sso7d-fusion polymerase, $MgCl_2$, EvaGreen dye and stabilizers) were run in white 96-well PCR plates Multiplate™ (Bio-Rad MLL9651). The qPCR program was as follows: step 1, 98 °C for 2 min; step 2, 90 °C for 5 s; step 3, 60 °C for 15 s; step 4, return to step 2 and repeat 40 times. At the end of the cycling program, a melting program (from 65 to 95 °C with a 0.5 °C increment every 5 s) was run to test the specificity of each qPCR. Data are expressed as fold enrichment at the HO-induced DSB relative to the non-cleaved *ARO1* locus, after normalizing ChIP signals to input at each time point. qPCR primers are listed in Supplementary Table 2.

Co-immunoprecipitation

Cells were lysed in 400 µl PBS 1X, 1% Triton X-100, 10% glycerol, EDTA 1 mM, NaF 10 mM, and protease inhibitor cocktail, as described[54]. Clarified extracts were incubated with 50 µL Protein A-Sepharose and 5 µg anti-HA for 2 h at 4 °C. Resins were washed three times with lysis buffer and three times with PBS 1X. Bound proteins were analyzed by Western blot using anti-Rad53 and anti-HA after separation on 10% SDS-PAGE.

In situ autophosphorylation (ISA) assay

Protein extracts prepared by TCA precipitation were loaded (25 µg per lane) on 10% SDS-PAGE, transferred to PVDF (Immobilon-P), and subjected to a denaturation/renaturation procedure, as described[35]. Denaturation: 7 M guanidine-HCl, 50 mM DTT, 2 mM EDTA, 50 mM Tris-HCl, pH 8.0, 1 h at room temperature. Membranes were washed twice in TBS (10 min each), then renatured at 4 °C for 12–18 h with gentle agitation in 2 mM DTT, 2 mM EDTA, 0.04% Tween-20, 10 mM Tris-HCl pH 7.5, 140 mM NaCl, 1% BSA. After a 60-min wash in 30 mM Tris-HCl pH 7.5 membranes were equilibrated in kinase buffer (1 mM DTT, 0.1 mM EGTA, 20 mM $MgCl_2$, 20 mM $MnCl_2$, 40 mM HEPES-NaOH pH 8.0, 100 µM sodium orthovanadate) for 30 min and incubated with [γ-^{32}P]ATP (10 µCi/mL) for 1 h at room temperature. Washes: 30 mM Tris-HCl pH 7.5 (10 min), 30 mM Tris-HCl pH 7.5 + 0.1% NP-40 (10 min), 30 mM Tris-HCl pH 7.5 (10 min), 1 M KOH (10 min), water (10 min), 10% TCA (10 min), water (10 min). Filters were dried and exposed.

Statistics and reproducibility

Statistical significance was evaluated with OriginPro software using unpaired, two-tailed Student's *t* tests. For Western blots, representative images are shown. Unless otherwise stated, 3 biological replicates were performed. A biological replicate is defined as an independent experiment using newly prepared biological material. No statistical methods were used to predetermine sample size; no samples or data points were excluded.

Reporting summary

Further information on research design is available in the Nature Portfolio Reporting Summary linked to this article.

Data availability

All data are available within the article and its Supplementary Information. Uncropped Western blots for Figs. 1A, C, D; 3A, C and 5B, D are shown in

Supplementary Figs. 6–10. Source data underlying Figs. 4B, C; 5A and 6A are provided as Supplementary Data. Additional information is available from the corresponding author upon reasonable request.

Received: 16 July 2025; Accepted: 12 December 2025;
Published online: 24 December 2025

References

1. Stinson, B. M. & Loparo, J. J. Repair of DNA double-strand breaks by the nonhomologous end joining pathway. *Annu. Rev. Biochem.* **90**, 137–164 (2021).
2. Mehta, A. & Haber, J. E. Sources of DNA double-strand breaks and models of recombinational DNA repair. *Cold Spring Harb. Perspect. Biol.* **6**, a016428 (2014).
3. Cejka, P. & Symington, L. S. DNA end resection: mechanism and control. *Annu. Rev. Genet.* **55**, 285–307 (2021).
4. Neale, M. J., Pan, J. & Keeney, S. Endonucleolytic processing of covalent protein-linked DNA double-strand breaks. *Nature* **436**, 1053–1057 (2005).
5. Shibata, A. et al. DNA double-strand break repair pathway choice is directed by distinct MRE11 nuclease activities. *Mol. Cell* **53**, 7–18 (2014).
6. Reginato, G., Cannavo, E. & Cejka, P. Physiological protein blocks direct the Mre11-Rad50-Xrs2 and Sae2 nuclease complex to initiate DNA end resection. *Genes Dev.* **31**, 2325–2330 (2017).
7. Wang, W., Daley, J. M., Kwon, Y., Krasner, D. S. & Sung, P. Plasticity of the Mre11–Rad50–Xrs2–Sae2 nuclease ensemble in the processing of DNA-bound obstacles. *Genes Dev.* **31**, 2331–2336 (2017).
8. Paull, T. T. & Gellert, M. The 3′ to 5′ exonuclease activity of Mre11 facilitates repair of DNA double-strand breaks. *Mol. Cell* **1**, 969–979 (1998).
9. Trujillo, K. M., Yuan, S. S., Lee, E. Y. & Sung, P. Nuclease activities in a complex of human recombination and DNA repair factors Rad50, Mre11, and p95. *J. Biol. Chem.* **273**, 21447–21450 (1998).
10. Hopfner, K. P. et al. Structural biochemistry and interaction architecture of the DNA double-strand break repair Mre11 nuclease and Rad50-ATPase. *Cell* **105**, 473–485 (2001).
11. Hopfner, K. P. et al. The Rad50 zinc-hook is a structure joining Mre11 complexes in DNA recombination and repair. *Nature* **418**, 562–566 (2002).
12. Deshpande, R. A., Lee, J. H. & Paull, T. T. Rad50 ATPase activity is regulated by DNA ends and requires coordination of both active sites. *Nucleic Acids Res.* **45**, 5255–5268 (2017).
13. Mimitou, E. P. & Symington, L. S. Sae2, Exo1 and Sgs1 collaborate in DNA double-strand break processing. *Nature* **455**, 770–774 (2008).
14. Zhu, Z., Chung, W. H., Shim, E. Y., Lee, S. E. & Ira, G. Sgs1 helicase and two nucleases Dna2 and Exo1 resect DNA double-strand break ends. *Cell* **134**, 981–994 (2008).
15. Keeney, S., Giroux, C. N. & Kleckner, N. Meiosis-specific DNA double-strand breaks are catalyzed by Spo11, a member of a widely conserved protein family. *Cell* **88**, 375–384 (1997).
16. Lobachev, K. S., Gordenin, D. A. & Resnick, M. A. The Mre11 complex is required for repair of hairpin-capped double-strand breaks and prevention of chromosome rearrangements. *Cell* **108**, 183–193 (2002).
17. Llorente, B. & Symington, L. S. The Mre11 nuclease is not required for 5′ to 3′ resection at multiple HO-induced double-strand breaks. *Mol. Cell. Biol.* **24**, 9682–9694 (2004).
18. Cannavo, E. & Cejka, P. Sae2 promotes dsDNA endonuclease activity within Mre11-Rad50-Xrs2 to resect DNA breaks. *Nature* **514**, 122–125 (2014).
19. Anand, R., Ranjha, L., Cannavo, E. & Cejka, P. Phosphorylated CtIP functions as a co-factor of the MRE11-RAD50-NBS1 endonuclease in DNA end resection. *Mol. Cell* **64**, 940–950 (2016).
20. Deshpande, R. A., Lee, J. H., Arora, S. & Paull, T. T. Nbs1 converts the human Mre11/Rad50 nuclease complex into an endo/exonuclease machine specific for protein–DNA adducts. *Mol. Cell* **64**, 593–606 (2016).
21. Williams, G. J. et al. ABC ATPase signature helices in Rad50 link nucleotide state to Mre11 interface for DNA repair. *Nat. Struct. Mol. Biol.* **18**, 423–431 (2011).
22. Möckel, C., Lammens, K., Schele, A. & Hopfner, K. P. ATP-driven structural changes of the bacterial Mre11 catalytic head complex. *Nucleic Acids Res.* **40**, 914–927 (2012).
23. Deshpande, R. A. et al. ATP-driven Rad50 conformations regulate DNA tethering, end resection, and ATM checkpoint signaling. *EMBO J.* **33**, 482–500 (2014).
24. Käshammer, L. et al. Mechanism of DNA end sensing and processing by the Mre11-Rad50 complex. *Mol. Cell* **76**, 382–394 (2019).
25. Gut, F. et al. Structural mechanism of endonucleolytic processing of blocked DNA ends and hairpins by Mre11-Rad50. *Mol. Cell* **82**, 3513–3522 (2022).
26. Colombo, C. V. et al. Functional and molecular insights into the role of Sae2 C-terminus in the activation of MRX endonuclease. *Nucleic Acids Res.* **52**, 13849–13864 (2024).
27. Nicolas, Y. et al. Molecular insights into the activation of Mre11-Rad50 endonuclease activity by Sae2/CtIP. *Mol. Cell* **84**, 2223–2237 (2024).
28. Ciccia, A. & Elledge, S. J. The DNA damage response: making it safe to play with knives. *Mol. Cell* **40**, 179–204 (2010).
29. Emili, A. MEC1-dependent phosphorylation of Rad9p in response to DNA damage. *Mol. Cell* **2**, 183–189 (1998).
30. Sun, Z., Hsiao, J., Fay, D. S. & Stern, D. F. Rad53 FHA domain associated with phosphorylated Rad9 in the DNA damage checkpoint. *Science* **281**, 272–274 (1998).
31. Vialard, J. E., Gilbert, C. S., Green, C. M. & Lowndes, N. F. The budding yeast Rad9 checkpoint protein is subjected to Mec1/Tel1-dependent hyperphosphorylation and interacts with Rad53 after DNA damage. *EMBO J.* **17**, 5679–5688 (1998).
32. Durocher, D., Henckel, J., Fersht, A. R. & Jackson, S. P. The FHA domain is a modular phosphopeptide recognition motif. *Mol. Cell* **4**, 387–394 (1999).
33. Schwartz, M. F. et al. Rad9 phosphorylation sites couple Rad53 to the *Saccharomyces cerevisiae* DNA damage checkpoint. *Mol. Cell* **9**, 1055–1065 (2002).
34. Sweeney, F. D. et al. *Saccharomyces cerevisiae* Rad9 acts as a Mec1 adaptor to allow Rad53 activation. *Curr. Biol.* **15**, 1364–1375 (2005).
35. Pellicioli, A. et al. Activation of Rad53 kinase in response to DNA damage and its effect in modulating phosphorylation of the lagging strand DNA polymerase. *EMBO J.* **18**, 6561–6572 (1999).
36. Gilbert, C. S., Green, C. M. & Lowndes, N. F. Budding yeast Rad9 is an ATP-dependent Rad53 activating machine. *Mol. Cell* **8**, 129–136 (2001).
37. Usui, T., Ogawa, H. & Petrini, J. H. A DNA damage response pathway controlled by Tel1 and the Mre11 complex. *Mol. Cell* **7**, 1255–1266 (2001).
38. Clerici, M., Mantiero, D., Lucchini, G. & Longhese, M. P. The *Saccharomyces cerevisiae* Sae2 protein negatively regulates DNA damage checkpoint signalling. *EMBO Rep.* **7**, 212–218 (2006).
39. Yu, T. Y., Kimble, M. T. & Symington, L. S. Sae2 antagonizes Rad9 accumulation at DNA double-strand breaks to attenuate checkpoint signaling and facilitate end resection. *Proc. Natl. Acad. Sci. USA* **115**, E11961–E11969 (2018).
40. Bonetti, D. et al. Escape of Sgs1 from Rad9 inhibition reduces the requirement for Sae2 and functional MRX in DNA end resection. *EMBO Rep.* **16**, 351–361 (2015).
41. Ferrari, M. et al. Functional interplay between the 53BP1-ortholog Rad9 and the Mre11 complex regulates resection, end-tethering and repair of a double-strand break. *PLoS Genet.* **11**, e1004928 (2015).

42. Gobbini, E. et al. Sae2 function at DNA double-strand breaks is bypassed by dampening Tel1 or Rad53 activity. *PLoS Genet.* **11**, e1005685 (2015).
43. Huertas, P., Cortés-Ledesma, F., Sartori, A. A., Aguilera, A. & Jackson, S. P. CDK targets Sae2 to control DNA-end resection and homologous recombination. *Nature* **455**, 689–692 (2008).
44. Huertas, P. & Jackson, S. P. Human CtIP mediates cell cycle control of DNA end resection and double strand break repair. *J. Biol. Chem.* **284**, 9558–9565 (2009).
45. Cannavo, E. et al. Regulatory control of DNA end resection by Sae2 phosphorylation. *Nat. Commun.* **9**, 4016 (2018).
46. Peterson, S. E. et al. Cdk1 uncouples CtIP-dependent resection and Rad51 filament formation during M-phase double-strand break repair. *J. Cell Biol.* **194**, 705–720 (2011).
47. Baroni, E., Viscardi, V., Cartagena-Lirola, H., Lucchini, G. & Longhese, M. P. The functions of budding yeast Sae2 in the DNA damage response require Mec1- and Tel1-dependent phosphorylation. *Mol. Cell. Biol.* **24**, 4151–4165 (2004).
48. Wang, H. et al. The interaction of CtIP and Nbs1 connects CDK and ATM to regulate HR-mediated double-strand break repair. *PLoS Genet.* **9**, e1003277 (2013).
49. Peterson, S. E. et al. Activation of DSB processing requires phosphorylation of CtIP by ATR. *Mol. Cell* **49**, 657–667 (2013).
50. Liang, J., Suhandynata, R. T. & Zhou, H. Phosphorylation of Sae2 mediates forkhead-associated (FHA) domain-specific interaction and regulates its DNA repair function. *J. Biol. Chem.* **290**, 10751–10763 (2015).
51. Yu, T. Y., Garcia, V. E. & Symington, L. S. CDK and Mec1/Tel1-catalyzed phosphorylation of Sae2 regulate different responses to DNA damage. *Nucleic Acids Res.* **47**, 11238–11249 (2019).
52. Pommier, Y., Sun, Y., Huang, S. N. & Nitiss, J. L. Roles of eukaryotic topoisomerases in transcription, replication and genomic stability. *Nat. Rev. Mol. Cell Biol.* **17**, 703–721 (2016).
53. Clerici, M., Mantiero, D., Lucchini, G. & Longhese, M. P. The *Saccharomyces cerevisiae* Sae2 protein promotes resection and bridging of double strand break ends. *J. Biol. Chem.* **280**, 38631–38638 (2005).
54. Colombo, C. V. et al. Uncoupling Sae2 functions in downregulation of Tel1 and Rad53 signaling activities. *Genetics* **211**, 515–530 (2019).
55. Lam, I. & Keeney, S. Mechanism and regulation of meiotic recombination initiation. *Cold Spring Harb. Perspect. Biol.* **7**, a016634 (2014).
56. Garcia, V., Phelps, S. E., Gray, S. & Neale, M. J. Bidirectional resection of DNA double-strand breaks by Mre11 and Exo1. *Nature* **479**, 241–244 (2011).
57. Manfrini, N., Guerini, I., Citterio, A., Lucchini, G. & Longhese, M. P. Processing of meiotic DNA double strand breaks requires cyclin-dependent kinase and multiple nucleases. *J. Biol. Chem.* **285**, 11628–11637 (2010).
58. Morin, I. et al. Checkpoint-dependent phosphorylation of Exo1 modulates the DNA damage response. *EMBO J.* **27**, 2400–2410 (2008).
59. Toczyski, D. P., Galgoczy, D. J. & Hartwell, L. H. CDC5 and CKII control adaptation to the yeast DNA damage checkpoint. *Cell* **90**, 1097–1106 (1997).
60. Pellicioli, A., Lee, S. E., Lucca, C., Foiani, M. & Haber, J. E. Regulation of *Saccharomyces* Rad53 checkpoint kinase during adaptation from DNA damage-induced G2/M arrest. *Mol. Cell* **7**, 293–300 (2001).
61. Cartagena-Lirola, H., Guerini, I., Viscardi, V., Lucchini, G. & Longhese, M. P. Budding yeast Sae2 is an in vivo target of the Mec1 and Tel1 checkpoint kinases during meiosis. *Cell Cycle* **5**, 1549–1559 (2006).
62. Liao, H. et al. Structure of the FHA1 domain of yeast Rad53 and identification of binding sites for both FHA1 and its target protein Rad9. *J. Mol. Biol.* **304**, 941–951 (2000).
63. Polato, F. et al. CtIP-mediated resection is essential for viability and can operate independently of BRCA1. *J. Exp. Med.* **211**, 1027–1036 (2014).
64. Liu, X. et al. CtIP is essential for early B cell proliferation and development in mice. *J. Exp. Med.* **216**, 1648–1663 (2019).
65. Casari, E. et al. The PP2A phosphatase counteracts the function of the 9-1-1 axis in checkpoint activation. *Cell Rep.* **42**, 113360 (2023).
66. Madeira, F. et al. The EMBL-EBI job dispatcher sequence analysis tools framework in 2024. *Nucleic Acids Res.* **52**, W521–W525 (2024).

Acknowledgements

We thank M. Resnick and J. Haber for providing yeast strains, M. Clerici for critical reading of the manuscript, and all the laboratory members for helpful discussion and comments. M.P.L. discloses support for the research of this work from Fondazione AIRC under IG 2022-ID. 27001 project and from the European Union-Next Generation EU, Mission 4 Component 2-CUP H53D23004770006.

Author contributions

M.P.L. conceived the study. E.C., M.G., and P.P. performed the experiments. R.T. performed bioinformatic analyses. M.P.L. supervised and coordinated the work. M.P.L. wrote the paper. E.C., M.G., P.P., and R.T. reviewed, commented and edited the manuscript.

Competing interests

The authors declare no competing interests.

Additional information

Supplementary information The online version contains supplementary material available at https://doi.org/10.1038/s42003-025-09424-7.

Correspondence and requests for materials should be addressed to Maria Pia Longhese.

Peer review information *Communications Biology* thanks Alessandro Sartori and the other anonymous reviewer(s) for their contribution to the peer review of this work. Primary handling editors: Valeria Naim and Christina Karlsson Rosenthal. A peer review file is available.